PAPER

Rheological behavior, crystallization properties, and foaming performance of chain-extended poly (lactic acid) by functionalized epoxy

Ming Li, [iD] [ab] Shengnan Li,[b] Bujin Liu, [iD] [ab] Tuanhui Jiang,[ab] Di Zhang,[ab] Lushuai Cao,[ab] Li He*[ab] and Wei Gong*[c]

The inherently linear poly (lactic acid) suffers unsatisfying foaming behavior due to its low melt strength and poor crystallization properties. To overcome this drawback, a random terpolymer of ethylene, acrylic ester and glycidyl methacrylate (EGMA) was employed to improve the rheological behavior, crystallization properties, and foaming performance of poly (lactic acid) (PLA) through a chain extension reaction. The branched/micro-crosslinked structure formed by the chain extension reaction between EGMA and PLA effectively improved the dynamic rheological properties of PLA. As the content of EGMA increased from 0 wt% to 20 wt%, the crystal nucleation and crystal growth rate of various PLA samples have been significantly accelerated, resulting in a larger number and smaller size of spherulites, and the crystallinity of various PLA samples increased from 7.9% to 38.54%. The cell size of various PLA foams decreased from 53.5 to 22.0 μm and the cell density increased from 3.5×10^6 cells per cm^3 to 2.5×10^7 cells per cm^3, meanwhile, the cellular morphology of PLA foam was obviously improved. Moreover, the actual weight loss of PLA foams reached 26.1%, which is higher than the theoretical weight loss.

1. Introduction

In recent years, due to the increasingly serious resource crisis and environmental pollution caused by traditional fossil-based non-degradable polymers, bio-based and biodegradable polymers have attracted more and more attention as green materials.[1,2] As a renewable resource-based aliphatic semicrystalline polyester, poly (lactic acid) (PLA) can be biodegraded and composted under favorable conditions.[3,4] Being a thermoplastic with properties that are comparable to some commodity polymers, it is viewed as a viable alternative to petroleum-sourced plastics. As part of the drive for renewable-source based products, thermoplastic foams made out of PLA have attracted considerable attention in sectors such as packaging, cushioning and thermal and sound insulation.[5,6] However, as a biodegradable aliphatic thermoplastic polyester, PLA exhibits some defects such as a linear molecular structure, low molecular weight, weak crystallization ability and low melt strength, which hinder its further application, especially in the foaming field.[7] Therefore, in order to obtain PLA foams with better foaming performance, PLA is usually necessary to be modified. Among many modification methods (chain extension, blending, filling,

etc.) which had been widely used in actual production, chain extension was one of the most effective methods.[8–13]

Wang X. *et al.*[5] employed poly (ethylene octene) grafted with glycidyl methacrylate (POE-g-GMA) to improve the rheological, thermal properties, toughness and foaming behaviors of poly (lactic acid) (PLA) through a chain extension effect, and prepared PLA foams with more regular cell morphology by supercritical CO_2 foaming. However, the cell size of the foams had not been reduced effectively and was still too large. Ying wei Di *et al.*[8] used 1,4-butane diisocyanate as a chain extender to increase the molecular weight of PLA through coupling and chain extension reactions to form a branched structure, and prepared PLA foam with small cell size and high cell density. Wei Liu *et al.*[14] prepared high foamability PLA resin by inducing chain extender through grafting octa(epox-ycyclohexyl) polyhedral oligomeric silsesquioxanes (POSS) on carbon nanotubes (CNT). In fact, chain extension can modify the crystallization behaviors of PLA, which improves the foaming behaviors of PLA by two aspects.[15] On the one hand, the generated crystals can be acted as physical cross-linking points, which is conducive to improve the melt strength and foamability of PLA as well as restrict the blowing agent gas loss and cell coalescence during the foaming process.[16] On the other hand, the interfaces between crystalline region and amorphous region can be treated as the heterogeneous nucleation sites for the cell nucleation to enhance cell density.[17] At the same time, chain extension can enhance the foamability of PLA by improving the viscoelasticity of PLA. Owing to foaming occur in the molten state, the melt strength of the

[a]*The Institute of Materials and Metallurgy of Guizhou University, Guiyang, China*
[b]*National Engineering Research Center for Compounding and Modification of Polymer Materials, Guiyang, China*
[c]*The Institute of Materials and Construction of Guizhou Normal University, Guiyang, China. E-mail: gongw@gznu.edu.cn; lihe@gzu.edu.cn*

resin is the main factor controlling the cell size.[18] The high melt viscosity is helpful to restrict the cell coalescence and rupture during cell growth stage, leading to the smaller cells.[19] The increase in melt viscoelasticity is beneficial to improve the foaming performance of PLA and increase the volume expansion rate (VER) of foamed PLA.[20] As explained above, chain extension is an effective way to improve the foaming performance of PLA.

At present, there is a little literature reported about the preparation of PLA foams by chemical injection foaming molding. Compared with autoclave foaming which is widely studied nowadays, chemical injection foaming molding is closer to actual production and application. However, some defects of PLA mentioned above usually cause poor foaming quality of PLA foams prepared by chemical injection foaming molding. Therefore, we selected ethylene-acrylic ester-glycidyl methacrylate terpolymer (EGMA) as an effective chain extender to modify the molecular weight and molecular chain structure of PLA, and prepared PLA foams containing different EGMA contents by chemical injection foaming molding. The effect of the addition of EGMA on the crystallization properties, rheological behavior and foaming performance of PLA was systematically studied. Besides, we analyzed the influence of EGMA on the foaming quality and weight loss of various PLA samples, and prepared PLA foams with uniform cell size and high cell density, which could provide guidance for the development of PLA industrialized foam products.

2. Experiment

2.1 Materials

Poly (lactic acid) (PLA), injection molding grade, was supplied by Anhui Fengyuan Futailai Polylactic Acid Co. Ltd. Ethylene-methyl acrylate-glycidyl methacrylate random terpolymer (EGMA, Lotader AX8900) with 8% glycidyl methacrylate ester (GMA) content was supplied by French Arkema company. The chemical structures and characteristics of the two materials are shown in Table 1. Azodicarbonamide (AC, gas emission 220 ml g^{-1}) was supplied by Wuhan Hanhong Chemical Plant. Zinc stearate (Zn(st)$_2$) was supplied by Wenzhou Jia Da Plastic Additives Co., Ltd. Zinc oxide (ZnO) was supplied by Xiangyun County Hongxiang Co., Ltd. LDPE (2426H) was supplied by Lanzhou Petrochemical Co. China, with the MFR of 1.8 g/10 min.
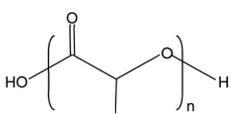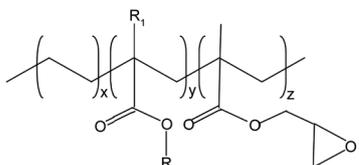
2.2 Sample preparation

2.2.1 AC foaming masterbatch preparation. In order to alleviate the effect of moisture, AC and LDPE were dried at 60 °C for 4 h before processing. Afterwards, they were melt blended in twin screw extruder (CTE35, Coperion Koryo Nanjing Machinery Co., Ltd Nanjing, China. The screw diameter was 35.6 mm and the length–diameter ratio was 36) with a LDPE/AC weight ratio of 90/10. The temperature of each section of the extruder from hopper to the die was set from 105 °C to 120 °C. The screw rotation speed was 200 rpm and the feeding speed was 18 rpm.

2.2.2 Foaming auxiliary masterbatch preparation. Zinc oxide (ZnO) and zinc stearate (Zn[St]$_2$) were dried at 60 °C for 4 h before processing. Zinc oxide (ZnO) and zinc stearate (Zn [St]$_2$) were evenly mixed at a mass fraction ratio of 7 : 3, then added to 90 parts of PLA evenly mixed.[21] The foaming auxiliary masterbatch was prepared by twin screw extruder (CTE35, it was the same as that used in the foaming masterbatch preparation) to extrude granulation. The temperature of each section of the extruder from hopper to the die was set from 155 °C to 170 °C. The screw rotation speed was 150 rpm and the feeding speed was 10 rpm. ZnO/Zn(St)$_2$ is a conventional activator of AC foaming agent, and the complexation between ZnO/Zn(St)$_2$ and AC foaming agent can effectively promote the activation and decomposition of foaming agent.

2.2.3 Preparation of PLA/EGMA blend. All the materials were dried at 60 °C for 8 h before processing. Then, EGMA was added to the base material PLA in different weight percentages (5 wt%, 10 wt%, 15 wt%, 20 wt%, 25 wt%). The proportioned sample was hand rolled evenly into a twin screw extruder (CTE35, it was the same as that used in the foaming masterbatch preparation) to extrude granulation. The temperature of each section of the extruder from hopper to the die was set from 155 °C to 170 °C. The screw rotation speed was 180 rpm and the feeding speed was 10 rpm.

2.2.4 Preparation of PLA/EGMA blending foam. The PLA/EGMA blend prepared above was dried at 80 °C for 8 h. Then, the matrix (PLA or PLA/EGMA), foaming masterbatch, and foaming auxiliary masterbatch are uniformly mixed according to 85 : 10 : 5 mass fraction ratio. The standard tensile samples were prepared by the microcellular injection-foaming molding machine (EM120-V, Zhen de plastic machinery Co., Ltd.

Table 1 Chemical structures and characteristics of PLA and EGMA used in this work

Agents	Chemical structures	Characteristics
PLA		Melt index (190 °C/2.16 kg): 13.3 g/10 min, melting point: 173.7 °C, density: 1.25 g cm^{-3}, M_W: 1.86 × 10^5 g mol^{-1}
EGMA		Glycidyl methacrylate content: 8% wt, methyl acrylate content: 24% wt, melt index (190 °C/2.16 kg): 6 g/10 min, melting point: 65 °C, density: 0.94 g cm^{-3}, M_W: 1.73 × 10^5 g mol^{-1}, epoxy equivalent: 1765 g mol^{-1}

Through the mold design, our research group modified the ordinary EM120-V injection molding machine and formed a characteristic microcellular injection-foaming molding machine for foaming.) using a core-back foam injection molding (FIM) technique. The temperature of each section of the injection machine from hopper to the die was set from 165 °C to 180 °C. The core-back distance was from 3.2 mm to 4.0 mm with the distance of micro-opening being 0.8 mm.

2.3 Characterizations

2.3.1 Fourier transform infrared spectra (FTIR). The PLA/EGMA blend was prepared into powder with a small saw blade, and then the KBr powder and the samples powder were ground and mixed uniformly at a mass ratio of 100 : 2. The mixed powder was pressed into a thin sheet with a diameter of 1 cm using a sampler. The infrared spectrometer (Nexus-6700, Nicolet, USA) was adopted to characterize the reaction between EGMA and PLA in the range of 4000–400 cm^{-1}.

2.3.2 Rheological measurements. Oscillatory shear rheological behavior was tested on a HAAKE Mars60 Rotational Rheometer (Thermo Fisher Scientific, USA) at 175 °C under a nitrogen atmosphere. The mold cavity volume was adjusted by core-back to prepare the samples with a thickness of 1.0 mm, and then a small circle with a diameter of 20 mm and a thickness of 1.0 mm were taken. Frequency sweep tests were subsequently performed at 175 °C to determine the dynamic properties of all samples in the frequency range from 0.05 to 100 Hz with a given strain amplitude of 1% (in order to ensure a linear viscoelasticity region in the tested polymer melt).

Uniaxial elongation rheological characterization was tested on a HAAKE Mars60 Rotational Rheometer (Thermo Fisher Scientific, USA) using the SER tool at 180 °C under a nitrogen atmosphere. The strain rate was 0.05 s^{-1} in this test. The mold cavity volume was adjusted by core-back to prepare a 1.0 mm thick spline, and then a small cuboid with a length of 25 mm, a width of 10 mm, and a thickness of 1.0 mm was taken for the uniaxial elongational viscosity tests. Before the rheological tests, all the samples were placed in the rheometer and heat to 180 °C and keep for 2 min to completely melt the sample.

2.3.3 Differential scanning calorimetry (DSC). Differential scanning calorimeter (DSC, TA Q25, New Castle, DE, USA) was employed to test the melting and crystallization parameters of samples under nitrogen atmosphere. The samples were first heated from 30 °C to 200 °C and held at 200 °C for 5 min in order to eliminate thermal history. The samples were then cooled to 30 °C at a rate of 10 °C min^{-1}, finally, heated again to 200 °C at the same rate. The crystallization and melting parameters were collected from the cooling and reheating scans. The degree of crystallinity (X_C) was calculated from the following eqn (1)

$$X_C = \frac{\Delta H_m - \Delta H_C}{\Delta H_0 \times w_{PLA}} \tag{1}$$

in which ΔH_m and ΔH_c were the enthalpies of melting and cold crystallization during the first heating cycle, respectively, and ΔH_0 (PLA) was the melting enthalpy (93.6 J g^{-1}) of assuming

100% crystalline PLA. W_{PLA} was the weight fraction of PLA in the PLA/EGMA blend.

2.3.4 Polarized optical microscope (POM). The spherulite micromorphology of diverse PLA specimens was observed at 120 °C via POM (BX-51, Olympus, Japan). Before observation of spherulite morphologies, each PLA specimen about 3 mg was fused on a heating stage for 5 min at 200 °C to eliminate its prior thermal history, cooled rapidly to 120 °C for the observation of the crystallization process.

2.3.5 Scanning electron microscopy (SEM). Scan electron microscopy (SEM, KYKY-EM6000) was used to investigate the cell morphology of foaming samples. A small notch was made in the middle of the foam sample, then cooled in liquid nitrogen for 3 h before cryogenically fracture. Finally, the foam samples were put into a vacuum drying oven at 80 °C for 4 h, and the foam sample cross section was sprayed with gold to observe the foam structure, and the corresponding SEM diagram was obtained. Cell size and cell density were obtained by Image Pro-plus software. The cell density (N), which referred to the number of cells per cubic centimeter of solid polymer, was determined from eqn (2):[17]

$$N = \left(\frac{n}{A}\right)^{\frac{3}{2}} v_f \tag{2}$$

where n was the number of cells in the scanning electron micrograph, A was the area of the micrograph (cm^2), and V_f was the volume expansion ratio (VER) of the foam, which could be calculated using eqn (3)

$$v_f = \frac{\rho_0}{\rho_f} \tag{3}$$

where ρ_0 and ρ_f were the apparent densities of samples before and after foaming process, which were measured by water displacement method according to XS205 DU-A2004002.

2.3.6 Weight loss. The American Mettler Toledo XS250 electronic analytical balance was used to test the apparent density of each sample according to DU-A2004002. Took five samples for each component to test and calculated the average density. Then used the following eqn (4) and (5) to calculate the weight loss of the foams:

$$W_0 = \frac{\Delta H}{H_1} \times 100\% \tag{4}$$

$$W_1 = \frac{\rho_0 - \rho_f}{\rho_f} \times 100\% \tag{5}$$

In the above formula, W_0 and W_1 (%) were theoretical and actual weight loss respectively, ΔH and H_1 (mm) were the distance of micro-opening and thickness of the foam sample respectively. where ρ_0 and ρ_f (g cm^{-3}) were the apparent densities of samples before and after foaming process.

3. Results and discussion

3.1 Structure analysis of chain-extended poly (lactic acid) (CPLA)

PLA has terminal hydroxyl and terminal carboxyl groups. EGMA is a ternary random copolymer of ethylene, acrylate and glycidyl
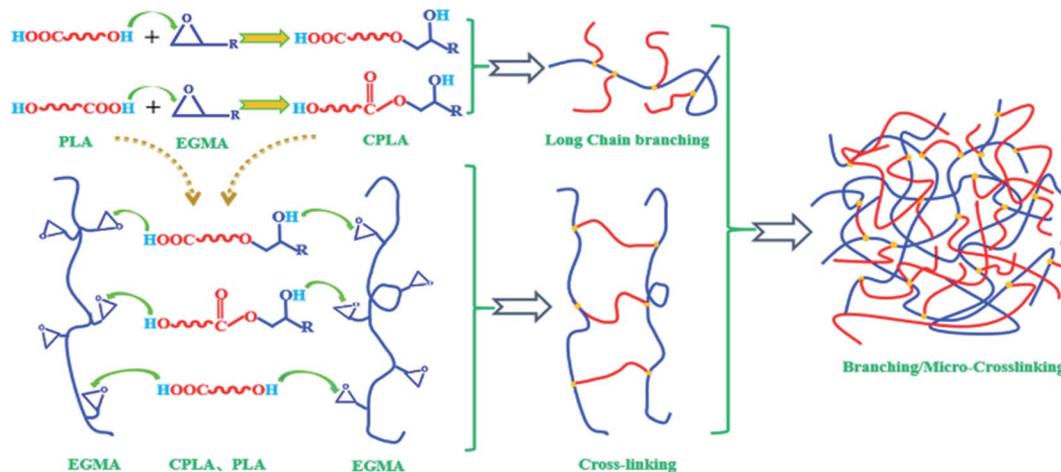
Fig. 1 Scheme of reaction between PLA and EGMA.

methacrylate. The epoxy groups on the EGMA side groups are reactive with –COOH and –OH in PLA. For this reason, adding a multifunctional epoxy compound for chain extension/branching reaction is conducive to obtaining chain-extended poly (lactic acid) (CPLA) with a long-chain branched structure. The reaction diagram between the terminal hydroxyl, terminal carboxyl and epoxy groups is shown in Fig. 1. When one end group of the PLA molecular chain reacts with EGMA, the other end group can also continue to participate in the reaction. In addition, whether the epoxy group reacts with the terminal hydroxyl group or the terminal carboxyl group, a new hydroxyl group will be generated. Therefore, the new group formed by the ring-opening reaction of PLA and the epoxy group still contains two active functional groups (one hydroxyl group and one carboxyl group or two hydroxyl groups), which can continue to react with the epoxy group on the EGMA. And the similar ring-opening reaction repeats constantly, which contributes to forming PLA with a branched/micro-crosslinked structure finally.

Fig. 2 shows the FTIR spectra of EGMA, pure PLA and CPLA. In Fig. 2(a), the characteristic absorption peaks of epoxy groups

at 721 cm^{-1} and 908 cm^{-1} could be observed for EGMA. Both characteristic peaks disappeared when EGMA was added to PLA, which indicated that the PLA/EGMA blend could undergo a series of reactions during the melt blending process, and the epoxy groups were consumed in the chain extension reaction between EGMA and PLA.[5,20] In Fig. 2(b), some characteristic peaks of PLA could be observed in the FTIR spectra of various PLA samples, which were the C=O vibration peak in the ester group at 1180 cm^{-1}, the C–H deformation vibration peak at 1455 cm^{-1}, and tensile vibration peak of C=O in ester group at 1750 cm^{-1}.[22] The C=O absorption peak of CPLA gradually enhanced with the increase of EGMA content, this could be attributed to more ester carbonyl groups (C=O) which were formed for the further intensification of the ring-opening chain extension reaction. In addition, only the chain-extended PLA had a characteristic peak at 2850 cm^{-1} that was related to the out-of-plane bending vibration of CH$_2$ in the ethylene segment of EGMA. It could be inferred that the reaction between PLA and EGMA had occurred successfully, and the modified PLA had formed branched/crosslinked molecular structure.[23]
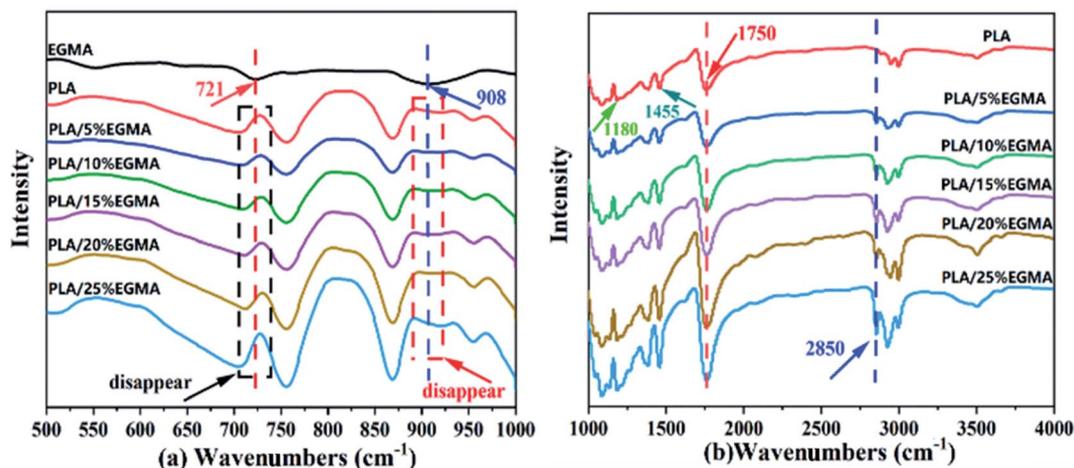

Fig. 2 FT-IR spectra of EGMA, pure PLA and CPLA. (a) 500–1000 cm^{-1} (b) 1000–4000 cm^{-1}.

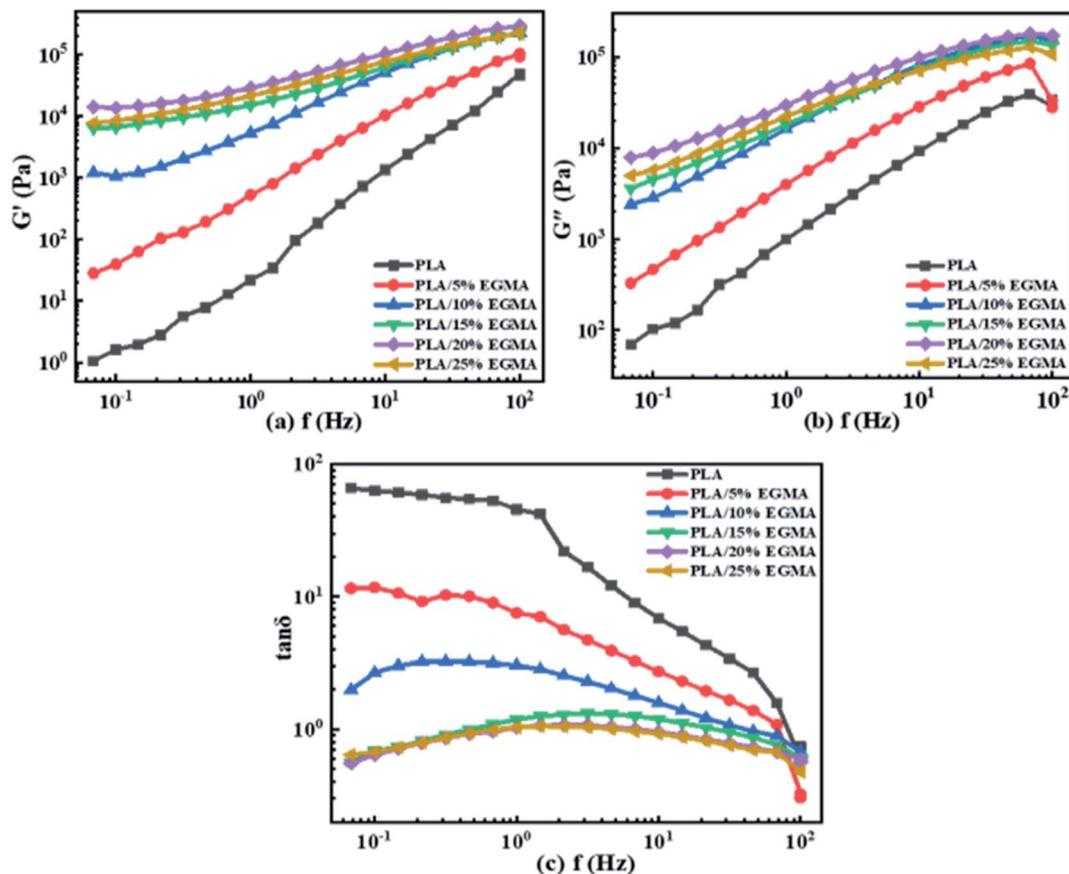© 2021 The Author(s). Published by the Royal Society of Chemistry

Fig. 3 Dynamic rheological properties of various PLA samples: (a) G' (b) G'' (c) tan δ.

3.2 Rheological behaviour

3.2.1 Viscoelasticity. Fig. 3 shows the dynamic rheological properties of various PLA samples with different EGMA content. In the test frequency range, the G' and G'' of various PLA samples gradually increased with the raise of EGMA content. However, G' and G'' would decrease as the content of EGMA continued to increase over 20 wt%. This could be attributed to

the agglomeration of excess EGMA in PLA, resulting in a decrease in the dispersibility of EGMA. The melt strength of polymer was considered to be highly related to the G' (characterizes melt elasticity) and G'' (characterizes the viscidity of the polymer), which was a crucial factor to judge the viscoelasticity of polymer.[5] PLA/EGMA blends with high melt elasticity could make cell to bear more intense tensile deformation to prevent
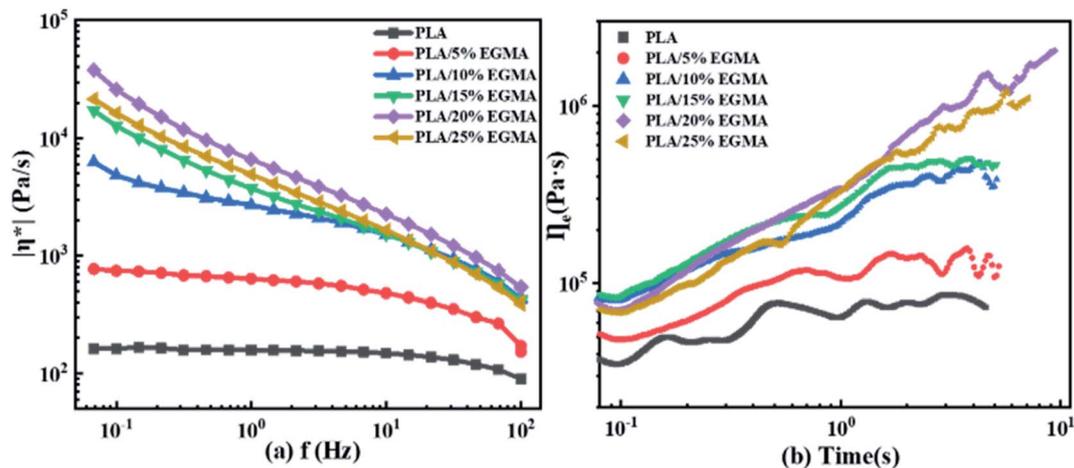

Fig. 4 Viscosity curves of various PLA samples: (a) complex viscosity (b) elongational viscosity.

cell rupture or cell collapse during cell growing process and ensured that nucleated bubbles eventually expanded to form regular cells.[20] Larger viscosity could ensure that the gas was evenly dispersed in the resin, which could prevent the uneven distribution of the gas in the resin due to gas aggregation, and avoided the cell size distribution interval is too wide. Therefore, greater elasticity could effectively make nucleated bubbles expand to form cells, and greater viscidity made gas easily diffuse in the matrix material to form uniform cells. After PLA was transformed from linear molecular chain structure to long-chain branched/micro-crosslinked structure, the formation of a large number of branches and micro-crosslinked networks leaded to the increase in the free volume between molecular chains and the enhancement of the movement ability of chain segments, but the relative slip between molecular chains was more difficult, which was reflected in the enhancement of polymer elasticity at the macro level. However, the severe entanglement and crosslinking network of molecular chains caused by branched/micro-crosslinked structure made the relative movement of molecular chains very difficult, and the movement ability of the whole molecular chain decreased sharply, which was reflected in the enhancement of polymer viscosity on the macro level. Therefore, we could say that the increase in elasticity and viscosity also confirmed the presence of branched/micro-crosslinked structures in PLA/EGMA blends. Fig. 3(c) shows the dependence of loss factor (tan δ) on f for diverse PLA specimens. The change in the elastic response of PLA/EGMA melt was represented by tan δ, which was defined as the ratio of G''/G'. The larger the tan δ, the greater the viscidity, and on the contrary the smaller the tan δ, the greater the elasticity.[24] Compared with G', tan δ value accurately reflected the factor of melt elastic response rather than the magnitude of melt elasticity.[25] With increasing EGMA concentration, the tan δ of various PLA samples gradually decreased at the entire measured f range. This phenomenon indicated that the elastic response of various PLA samples became faster, and their viscous dissipation gradually decreased, which caused their foamability could be enhanced effectively. This was owing to the

increment in number of entanglement points for various PLA samples after chain extension, and those entanglement points could be acted as the physical network sites to enhance the melt elasticity of PLA/EGMA blend.[26]

3.2.2 Complex viscosity and elongational viscosity. The complex viscosity and elongational viscosity curves of various PLA samples are shown in Fig. 4(a) and (b). It could be seen from Fig. 4(a) that the complex viscosities of various PLA samples gradually increased as the EGMA content increased, and the complex viscosities of the CPLA would appear obvious shear thinning with the increase of the shear rate, but pure PLA would not be like this. This was because pure PLA was mainly a linear long-chain structure, and the viscosity would not change significantly with the shear rate. However, chain-extended PLA had a large number of molecular entanglements due to the branched/cross-linked structure, which made their viscosities increase significantly. When the shear rate increased, the molecular chains in the chain-extended PLA were untangled or even broken, resulting in a more obvious decrease in viscosity.[8] As displayed Fig. 4(b), under the strain rate of 0.05 s^{-1}, the introduction of EGMA caused PLA to appear strain hardening, and the tensile viscosities increased significantly with time. This was due to the increased molecular chain entanglement associated with branching/crosslinking structure hindering chain contraction during extension, resulting in obvious strain hardening behavior.[27] Therefore, EGMA could not only improve the response speed of viscoelasticity of PLA by chain extension reaction, but also increased the complex viscosity and tensile viscosity of PLA, so that the CPLA exhibited a better visco-elastic effect and higher tensile strength during melting. The higher melt strength of CPLA could effectively inhibit the merger, rupture of the cells and gas escape during the foaming process,[20] and achieved the purpose of improving the foaming quality.

3.3 Crystallization properties

The DSC curves and thermal parameters of various PLA samples are plotted in Fig. 5 as well as compared in Table 2, respectively. Fig. 5 revealed that the cooling crystallization peak of various
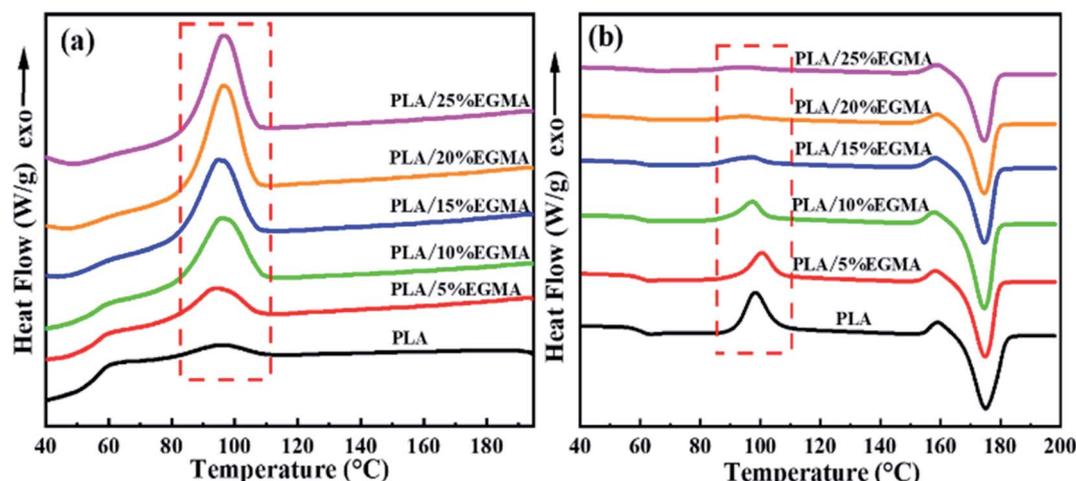

Fig. 5 DSC curve of various PLA samples: (a) cooling curves (b) heating curves.

Table 2   Thermal parameters of various PLA samples

Sample	T_g (°C)	T_c (°C)	T_m (°C)	ΔH_c (J g^{-1})	ΔH_m (J g^{-1})	X_C (%)
PLA	59.40	98.42	175.04	35.38	42.77	7.90
PLA/5%EGMA	59.23	100.70	174.85	23.07	37.33	16.04
PLA/10%EGMA	58.92	98.05	174.34	18.47	38.89	24.24
PLA/15%EGMA	60.34	97.66	174.74	9.75	36.56	33.70
PLA/20%EGMA	60.34	95.07	174.66	4.43	33.29	38.54
PLA/25%EGMA	60.41	94.43	174.65	4.89	31.34	37.67

PLA samples gradually increased with the increase of EGMA, and the cold crystallization peak of heating curves gradually decreased, as a result, the crystallinity of various PLA samples gradually increased from 7.90% to 38.54%. This is because pure PLA is a semi-crystalline polymer with poor crystallization ability and slow crystallization rate. As for CPLA, the branching degree of CPLA increased as the chain extension reaction intensified, and a large number of branch points could be treated as heterogeneous nucleation sites of CPLA crystals. The branched structure enhanced the nucleation ability of CPLA crystals and improved the crystallinity.[5] However, as the EGMA content continued to increase from 20% to 25%, the X_C (crystallinity) of the CPLA samples dropped from 38.54% to 37.67%. This was owing to the excessive gel formed in the CPLA sample, which restricted the nucleation and growth of CPLA crystals.[7] The improvement of crystallization properties could ameliorate the foaming performance of PLA from two aspects: on the one hand, the generated crystals could be acted as physical cross-linking points, which was conducive to improve the melt strength and foamability of CPLA as well as restricted the blowing agent gas loss and cell coalescence during the foaming process.[16] On the other hand, the interfaces between crystalline region and amorphous region could be treated as the heterogeneous nucleation sites for the cell nucleation to enhance cell density.[17]

3.4   POM observation

POM was utilized to check the spherulite growth rate and morphology of diverse PLA specimens isothermally crystallized at 120 °C and the corresponding POM micrographs were exhibited in Fig. 6. Well-defined spherulites with representative Maltese cross were observed in the POM images of diverse PLA specimens, revealing a typical homogeneous crystallization nucleation.[28] It was noteworthy that the crystallite structure and crystallization kinetics of the pure PLA and CPLA were quite different. In the pure PLA, several minutes were required for the nucleation with only a small number of crystals, and these crystals grew very slowly. With the EGMA presence, both the crystal nucleation and the crystal growth rates dramatically accelerated, thus, a greater number of crystals, which were smaller, were created in the CPLA. This was attributed to the formation of branching structures which could be acted as the points of crystallization nucleation to enhance the number of spherocrystals after chain extension.[29] Meanwhile, the mobility of PLA molecular chains was reduced by the formation of branching structures, which would hinder PLA molecular chains moving into the crystal lattice and limit spherocrystal growth.[30] In summary, the generation of branching structure had double effects on the crystallization of PLA. The formation of branching structures in CPLA was favorable for crystallization nucleation and disadvantageous for crystallization growth, resulting in the generation of a large number of small spherocrystals in CPLA.[31] The cross-linked network formed by many small and dense crystals as physical cross-linking points could effectively improve the melt strength of PLA. It could be also found that the changes in crystallization properties observed by POM were consistent with the DSC test results.
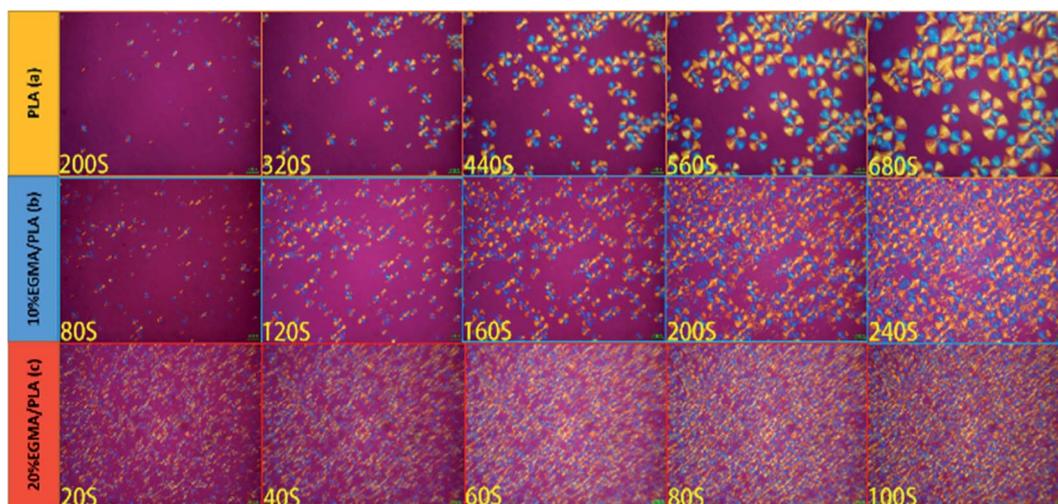

Fig. 6   POM images of various PLA samples isothermally crystallized at 120 °C: (a) pure PLA, (b) PLA/10%EGMA, (c) PLA/20%EGMA.
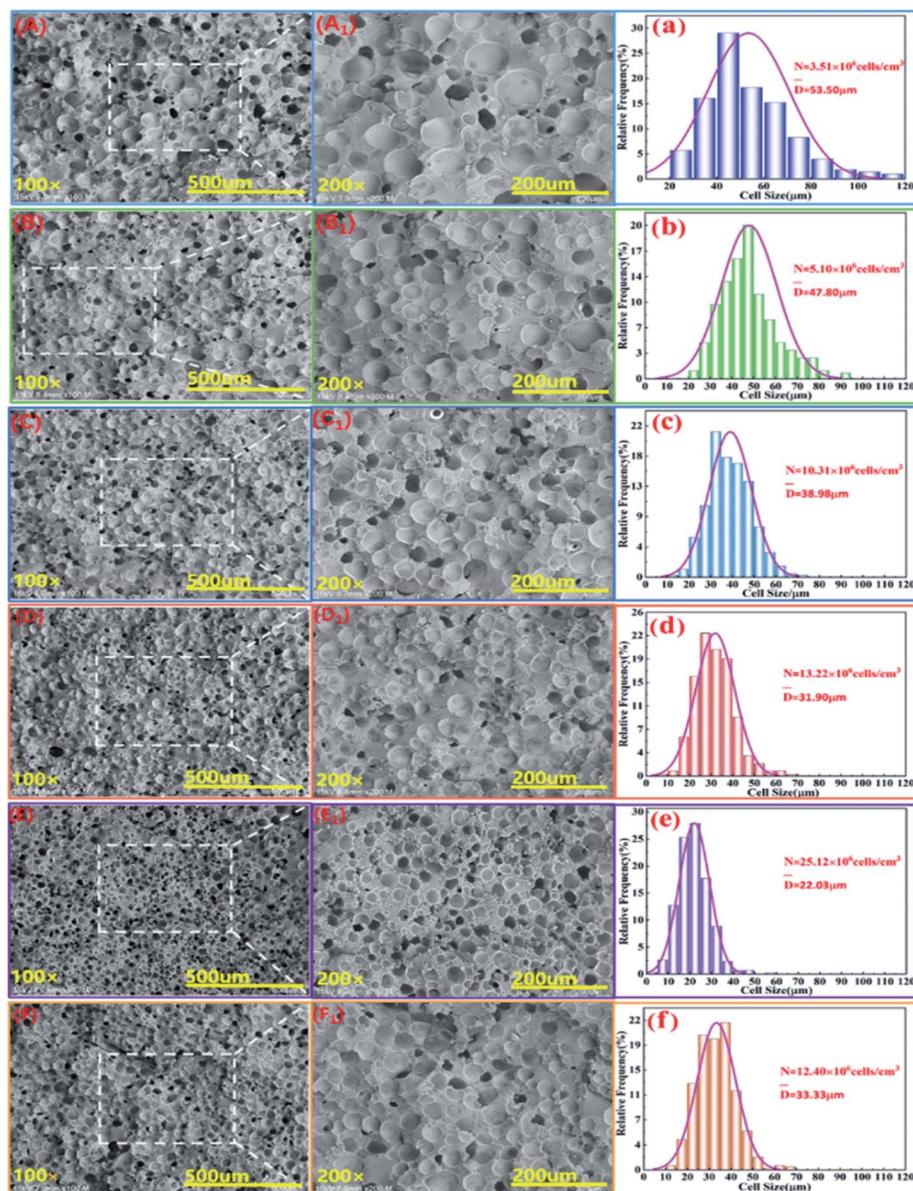
Fig. 7 SEM micrographs (A–F: ×100, A₁–F₁: ×200) and cell size distribution (a–f) of various PLA foams, EGMA mass fraction: (A) 0 wt%; (B) 5 wt%; (C) 10 wt%; (D) 15 wt%; (E) 20 wt%; (F) 25 wt%.

3.5 Foaming performance of various PLA foams

Fig. 7 shows the cell structure and cell diameter distribution of various PLA foams with different EGMA contents. The corresponding average diameter and cell density are shown in Fig. 8. It could be found that the cells of pure PLA foam were larger and deformed seriously with the average cell size of about 53.5 μm, the cell density about 3.1×10^6 cells per cm^3, and wider the cell size distribution (Fig. 7(a)).

These findings could be attributed to the low melt strength and poor crystallization properties of pure PLA. The normal distribution curve of cell diameter of various PLA foams gradually shifted to the low value area of the X axis when the mass fraction of EGMA increased from 0% to 20%, which responded the average cell diameter of various PLA foams gradually

decreased from 53.5 μm to 22.03 μm, meanwhile, the cell density increased from 3.51×10^6 cells per cm^3 to 25.12×10^6 cells per cm^3 and the cell distribution became more uniform. Compared with the pure PLA, CPLA significantly improved the foam morphology with smaller cell size to provide regular cells. At the same time, the density of the cell increased and the distribution narrowed (Fig. 7(b–f)), especially when the addition amount of EGMA was 20 wt%. After which the EGMA content continued to increase excessively, the average cell size increased and the cell density decreased greatly with the foaming quality beginning to deteriorate (see Fig. 7F1). This was mainly due to the fact that the addition of EGMA not only improved the crystallization properties of PLA, but also made a large number of heterogeneous nucleation sites form between the crystalline
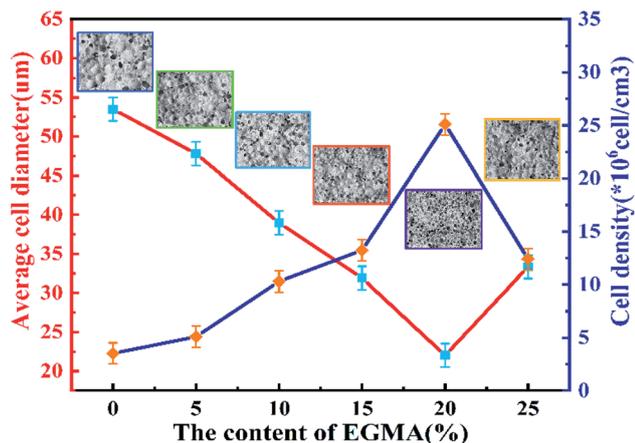
Fig. 8 Variations of average cell diameter and cell density of various PLA foams.

Fig. 10 Cell-forming processes in microcellular injection molding: (a) early filling stage; (b) mid filling stage; (c) after micro opening.

region and the amorphous region to effectively increase the cell density. Meanwhile, EGMA enhanced greatly the melt strength of CPLA (see the analysis and discussion part of Fig. 3 and 4), so that the bubble core could expand to form cells, and larger stress was generated on the cell wall during the cell growth stage, which could inhibit the rapid growth of the cells and reduce the phenomenon of cell deformation, rupture and coalescence.[32] As a result, we could obtain PLA foams with uniform cell size and high cell density.

Fig. 9 shows single cell structures (×2K) of pure PLA foam and PLA/20%EGMA foam. It could be observed from Fig. 9 that the cell of pure PLA foam had undergone obvious deformation which was like ellipsoid, and there were a lot of rough wrinkles on the cell wall, while the cell morphology of PLA/20%EGMA foam tended to be more regular spheres, and the cell wall was smoother and flatter. On the one hand, melt elasticity was the key factor to control cellular morphology during the growth of cells. High melt elasticity could withstand the stretching force during cell growing process, and ensured that the gas in the bubble expanded evenly around, while avoiding cell rupture or serious cell collapse during cell growing process, so that the cellular morphology became more regular.[33] On the other hand, the poor crystallization performance of pure PLA resulted in
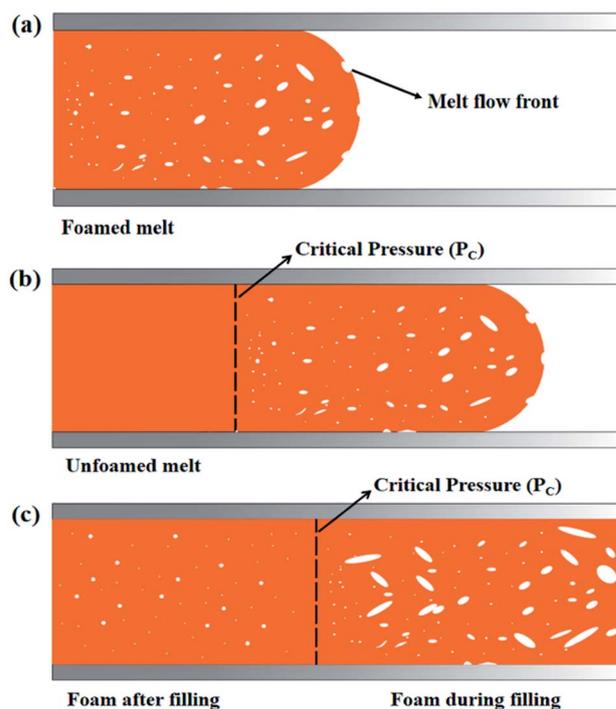
slow formation and uneven distribution of crystal regions, which would cause uneven shrinkage of the resin on the cell wall during the foam cooling and molding process, resulting in the formation of a large number of wrinkles on the cell wall and deformed cells. However, the rapid formation of dense and uniform crystal regions in the PLA/20%EGMA composites could make the bubble stable quickly and prevent the cells from deforming significantly, thereby forming a more regular cell morphology that tends to be spheres.

3.6 Weight loss behavior of various PLA foams

In our previous studies, we had found that there were two cell forming processes, "foam during filling" process and "foam after filling" process, in microcellular injection-molding
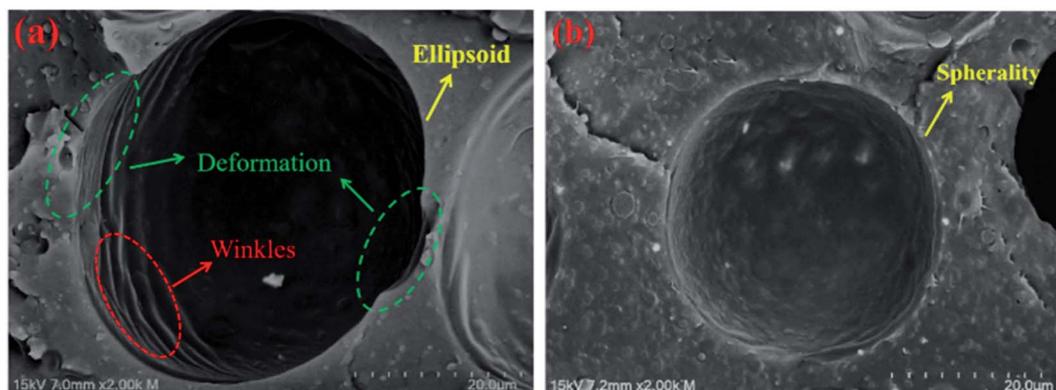

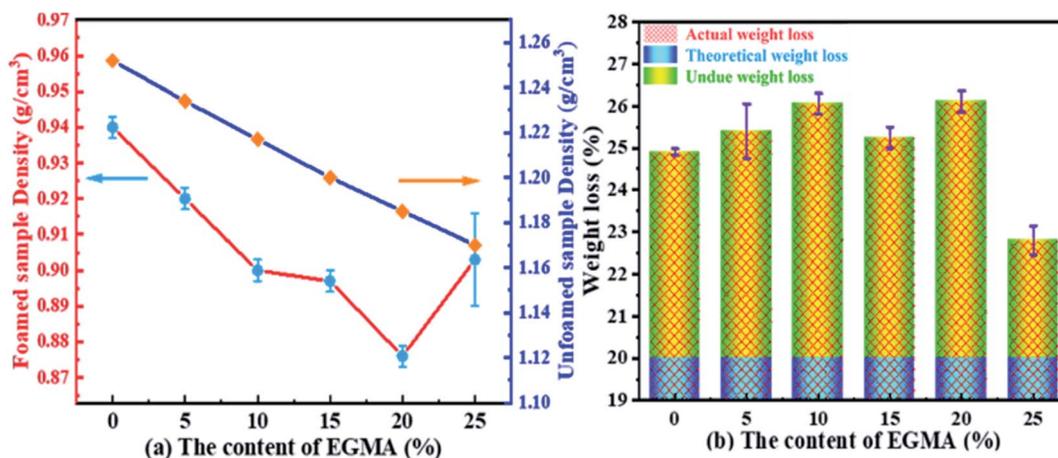Fig. 9 Single cell structures (×2K) of pure PLA foam and PLA/20%EGMA foam.

Fig. 11 Average densities and weight loss of various PLA foams: (a) sample density (g cm^{-3}), (b) weight loss (%).

process, and the melt pressure in the filling stage was the dominant factor affecting the cell forming processes. In filling stage, the melt near the flow front with a pressure lower than a critical pressure value would foam during filling. But the melt near the gate with a pressure higher than the critical pressure value would not foam during filling, and it foamed in cooling stage after filling stage.[34] "Foam during filling" would lead to excessive weight loss. These two kinds of cell forming processes in microcellular injection molding were shown in Fig. 10.

The average densities of various PLA foams and its weight loss range are shown in Fig. 11. From Fig. 11(a), it could be seen that the densities of the various PLA foams gradually decreased with the increase of EGMA. It was because the densities of pure PLA and EGMA were 1.252 g cm^{-3} and 0.94 g cm^{-3} respectively, and the density of EGMA was less than pure PLA. Therefore, the densities of various PLA samples decreased in an orderly manner as the EGMA content gradient increased, and the downward trend was almost a slope fixed straight line. The densities of CPLA foams decreased to 0.876 g cm^{-3} with the EGMA content increasing from 0% to 20%, after which the densities of CPLA foams increased with the EGMA content continuing to rise. This was because the densities of CPLA foams were not only affected by the relative content of PLA and EGMA, but also by the foaming quality. The melt strength of PLA/EGMA blend increased as the content of EGMA raised, which could effectively restrict the overgrowth, merging and rupture of cells and reduced gas escape during the foaming process,[27] and foaming quality was significantly improved, thereby the densities of CPLA foams was further reduced. However, the foaming quality of CPLA foams would decrease and the densities the CPLA foams increased when EGMA was overmuch.

Fig. 11(b) indicated that the actual weight loss of all PLA foams were greater than the theoretical weight loss. This was due to the fact that there would be in the formation of cells when the melt was in the process of filling the cavity (Fig. 10(a and b), "foam during filling" process, which caused the melt filled into the cavity was not dense before the micro-molding,

but partially foamed resin.[35] The actual injection volume of the injection molding machine was less than the theoretical injection volume, which resulted in the actual weight loss generally greater than the theoretical weight loss. Fig. 11(b) also indicated that the actual weight loss of the various PLA foams increased from 24.9% to 26.1% as the content of EGMA increased from 0% to 20%, after that, the weight loss decreased with the EGMA content continuing to increase. This attributed to the fact that the melt pressure would gradually increase during the filling process, and the lower melt strength of the resin would bring about the lower ability to confine gas, which caused the generated cells were more likely to deform, merge, rupture and finally gas escaped. As a result, resin injected in the filling stage was denser and injection volume of the injection machine increased, so that the weight loss of the foamed sample was reduced. However, increasing melt strength of PLA could make the phenomenon of cell rupture and gas escape during the filling stage improved by addition of EGMA, so that the number of cells and gas content in the resin was greater and the actual injection volume of the injection molding machine was less, which caused the weight loss of various PLA foams were greater finally. But the melt strength of PLA/EGMA blend would decrease when EGMA was overmuch, and the number of cells and gas content in the resin during the filling stage would also decrease, which resulted in an increase in the injection volume and a decrease in weight loss.

4. Conclusions

In this paper, PLA/EGMA blending foams were prepared by the melt blending and chemical injection foaming. Due to the branched/micro-crosslinked structure between PLA and EGMA, the viscoelasticity and complex viscosities of various PLA samples were significantly improved, and this structure imparted conspicuous strain-hardening behavior to the PLA melts. At the same time, a large number of branching sites in PLA after chain extension could be acted as nucleation sites for crystallization, which significantly increased the crystallization rate and spherulite density of PLA, while reducing spherulite

size. The obvious improvement of rheological behavior and crystallization properties of PLA provided a great environment for the growth and shaping of cells, which helped to form the cell structure with smaller size, greater density and more regular morphology, thus achieving the purpose of improving the foaming performance. In addition, the weight loss behavior of PLA foams was affected by foaming performance, and excellent foaming performance would lead to greater weight loss. Based on the above research, we obtained a simple and effective method to improve PLA foaming quality, which would provide some guidance for the development of PLA injection foaming molding products.

Conflicts of interest

There are no conflicts to declare.

Acknowledgements

References

1 B. Qi, Z. M. Xu, T. Liu and L. Zhao, *Polym. Mater. Sci. Eng.*, 2010, **26**, 138–141.
2 H. Tsuji and I. Fukui, *Polymer*, 2003, **44**, 2891–2896.
3 J. R. Rocca-Smith, R. Pasquarelli, A. Lagorce-Tachon, J. Rousseau, S. Fontaine, V. Aguié-Béghin and T. Karbowiak, *ACS Sustainable Chem. Eng.*, 2019, **7**, 3759–3771.
4 L. T. Lim, R. Auras and M. Rubino, *Prog. Polym. Sci.*, 2008, **33**, 820–852.
5 X. Wang, J. Mi, J. Wang, H. Zhou and X. Wang, *RSC Adv.*, 2018, **8**, 34418–34427.
6 M. Nofar and C. B. Park, *Prog. Polym. Sci.*, 2014, **39**, 1721–1741.
7 H. Zhou, M. Zhao, Z. Qu, J. Mi, X. Wang and Y. Deng, *J. Polym. Environ.*, 2018, **26**, 3564–3573.
8 Y. Di, S. Iannace, E. Di Maio and L. Nicolais, *Macromol. Mater. Eng.*, 2005, **290**, 1083–1090.
9 S. Pilla, A. Kramschuster, J. Lee, C. Clemons, S. Gong and L. S. Turng, *J. Mater. Sci.*, 2010, **45**, 2732–2746.
10 K. Li, Z. Cui, X. Sun, L. S. Turng and H. Huang, *J. Biobased Mater. Bioenergy*, 2011, **5**, 442–451.
11 H. Zhao, G. Zhao, L. S. Turng and X. Peng, *Ind. Eng. Chem. Res.*, 2015, **54**, 7122–7130.
12 S. Pilla, A. Kramschuster, S. Gong, A. Chandra and L. S. Turng, *Int. Polym. Process.*, 2007, **22**, 418–428.
13 M. Mihai, M. A. Huneault and B. D. Favis, *Polym. Eng. Sci.*, 2010, **50**, 629–642.
14 W. Liu, X. Zhu, H. Gao, X. Su and X. Wu, *Cell. Polym.*, 2020, **39**, 117–138.
15 M. Mihai, M. A. Huneault and B. D. Favis, *J. Appl. Polym. Sci.*, 2009, **113**, 2920–2932.
16 J. Wang, W. Zhu, H. Zhang and C. B. Park, *Chem. Eng. Sci.*, 2012, **75**, 390–399.
17 K. Taki, D. Kitano and M. Ohshima, *Ind. Eng. Chem. Res.*, 2011, **50**, 3247–3252.
18 P. Tiwary, C. B. Park and M. Kontopoulou, *Eur. Polym. J.*, 2017, **91**, 283–296.
19 T. R. Kuang, H. Y. Mi, D. J. Fu, X. Jing, B. Y. Chen, W. J. Mou and X. F. Peng, *Ind. Eng. Chem. Res.*, 2015, **54**, 758–768.
20 J. Song, J. Mi, H. Zhou, X. Wang and Y. Zhang, *Polym. Degrad. Stab.*, 2018, **157**, 143–152.
21 B. Liu, T. Jiang, X. Zeng, R. Deng, J. Gu, W. Gong and L. He, *Polym. Adv. Technol.*, 2021, **32**, 2102–2117.
22 S. Milovanovic, D. Markovic, A. Mrakovic, R. Kuska, I. Zizovic, S. Frerich and J. Ivanovic, *Mater. Sci. Eng., C*, 2019, **99**, 394–404.
23 B. Xue, H. He, Z. Zhu, J. Li, Z. Huang, G. Wang and Z. Zhan, *Polymers*, 2018, **10**, 1401.
24 C. Wang, H. Duan, C. Zhang, T. Jiang, H. Li and G. Wei, *Polym. Mater. Sci. Eng.*, 2016, **32**, 131–136.
25 W. Liu, X. Wu, Y. Ou, H. Liu and C. Zhang, *E-Polymers*, 2021, **21**, 96–107.
26 Y. Li, J. Mi, H. Fu, H. Zhou and X. Wang, *ACS Omega*, 2019, **4**, 12512–12523.
27 N. Najafi, M. C. Heuzey, P. J. Carreau, D. Therriault and C. B. Park, *Rheol. Acta*, 2014, **53**, 779–790.
28 J. Ramontja, S. S. Ray, S. K. Pillai and A. S. Luyt, *Macromol. Mater. Eng.*, 2009, **294**, 839–846.
29 Y. Yang, X. Li, Q. Zhang, C. Xia, C. Chen, X. Chen and P. Yu, *J. Supercrit. Fluids*, 2019, **145**, 122–132.
30 M. Buccella, A. Dorigato, E. Pasqualini, M. Caldara and L. Fambri, *Polym. Eng. Sci.*, 2014, **54**, 158–165.
31 L. Wei, H. Shicheng and Z. Hongfu, *J. Appl. Polym. Sci.*, 2018, **135**, 46399.
32 G. Wang, J. Zhao, K. Yu, L. H. Mark, G. Wang, P. Gong and G. Zhao, *Polymer*, 2017, **119**, 28–39.
33 W. Liu, S. He and Y. Yang, *Polym. Int.*, 2019, **68**, 516–526.
34 G. Dong, G. Zhao, Y. Guan, G. Wang and X. Wang, *J. Appl. Polym. Sci.*, 2014, **131**, 383–390.
35 G. Dong, G. Zhao, Y. Guan, S. Li and X. Wang, *J. Cell. Plast.*, 2016, **52**, 419–439.